ORNL/SPR-2021/1891

Technology Enabling Zero-EPZ Micro Modular Reactors

Milestone M3.1.1

Downselection of Cladding Materials for Zirconium Hydride Moderator

Principal Investigator: Jason R. Trelewicz
Award Number: DE-AR0000977
Prime Recipient: Stony Brook University
Sub-recipients: University of Tennessee Knoxville Oak Ridge National Laboratory
Project Period: 03/13/2019 – 09/12/2021
Milestone report #: 3.1.1
Milestone authors: Xunxiang Hu (ORNL) Briana Hiscox (ORNL) Benjamin R. Betzler (ORNL) Ying Yang (ORNL) Omer Karakoc (ORNL) Yutai Katoh (ORNL)
Due date: 03/12/2021
Report submission date: 03/12/2021

SUMMARY

This report complete Milestone M3.1.1 — "*Cladding downselection: Team will report to ARPA-E on at least two down-selected cladding options—one metallic and one ceramic.*" In this milestone, we systematically assess FeCrAl alloys and SiC-based cladding options for a zirconium hydride (ZrHx) moderator in terms of their neutronics, radiation stability, hydrogen permeability, chemical compatibility, and fabricability. The analysis shows that FeCrAl alloys are excellent candidate cladding materials for a ZrHx moderator given their proven radiation stability, acceptable compatibility with ZrHx, and industrially established fabricability. The relative high hydrogen permeability is manageable by introducing a thin layer of an Al_2O_3 hydrogen permeation barrier on the external surface. The SiC-cladded ZrHx moderator is promising because of its outstanding neutronics performance, excellent radiation stability, and extremely low intrinsic hydrogen permeability. However, potential interactions of SiC and Zr and the challenge in achieving a hermetic SiC-based cladding require further investigation.

CONTENTS

Summary ii
Acronyms v
Acknowledgments vi
1 Introduction 1
2 Reactor physics analysis of cladding materials for zirconium hydride moderator 4
2.1 Criticality evaluation of selected cladding materials 4
2.2 Cycle length calculation 5
2.3 Neutron flux spectra 5
3 FeCrAl cladding 7
3.1 Hydrogen permeability 7
3.2 Chemical compatibility of FeCrAl with ZrHx 8
3.3 Radiation stability 10
3.4 Fabricability 11
4 SiC-based cladding 12
4.1 Hydrogen permeability 12
4.2 Chemical compatibility of SiC with ZrHx 13
4.3 Radiation stability 14
4.4 Fabricability 15
5 Summary 17
6 References 18

FIGURES

Figure 1. k_{eff} as a function of fuel volume fraction for a 1-meter reflected spherical reactor core showing only hydrogen-bearing moderators yield increased reactivity when fuel is displaced [10]. 2
Figure 2 (a). Hydrogen desorption flux from a $ZrH_{1.62}$ disk (surface area of 18 mm^2, thickness of 0.6 mm) as a function of time during heating process. (b) Schematic illustration of the concentration profile during the dehydriding process [13]. 3
Figure 3. HTGR cycle length of the evaluated cladding materials. 5
Figure 4. Beginning-of-cycle neutron flux normalized per unit of lethargy 6
Figure 5. End-of-cycle neutron flux normalized per unit of lethargy. 6
Figure 6. Arrhenius plot of the hydrogen permeability for T35Y1, T54Y2, APMT, 304SS, 406SS, Zircaloy-2, Zircaloy-4, and pure iron over a temperature range from 350 to 650°C [20]. 8

Figure 7. Mole fraction of the formed phases as a function of temperature for the Fe-Cr-Al-H-Zr system 9
Figure 8. Mole fraction of the formed phases as a function of temperature for the Zr-H-Al-O system. 10
Figure 9. Arrhenius plot of the hydrogen permeability for SiC and selected ceramic materials [38] 13
Figure 10. Mole fraction of the formed phases as a function of temperature for the Si-C-H-Zr system 14
Figure 11. The first-generation SiC samples fabricated by laser-powder bed fusion additive manufacturing. The cylinders are of 0.5 in. (12.7 mm) outer diameter. 16
Figure 12. X-ray diffraction spectrum taken from Specimen A3 of femtosecond laser-manufactured SiC, indicating the presence of multiple SiC polytypes and metallic silicon. 17

TABLES

Table 1. Optimal volume fractions of components that result in the highest reactivity. 4
Table 2. Chemical compositions (wt %) of the alloys used for permeation tests [20]. 8

ACRONYMS

Al	Aluminum
Al_2O_3	Aluminum oxide
ARPA-E	Advanced Research Projects Agency-Energy
ATF	Accident-tolerant fuel
Cr	Chromium
CVD	Chemical vapor deposition
CVI	Chemical vapor infiltration
dpa	Displacement per atom
EFPD	Effective full power days
Fe	Iron
H	Hydrogen
HTGR	High-temperature gas-cooled reactor
LWR	Light water reactor
MEITNER	Modeling-Enhanced Innovations Trailblazing Nuclear Energy Reinvigoration
Mo	Molybdenum
ORNL	Oak Ridge National Laboratory
RT	Resource Team
SCC	Stress corrosion cracking
SiC	Silicon carbide
SiC/SiC	SiC fiber–reinforced SiC matrix composite
XRD	X-ray diffraction
YSZ	Yttria-stabilized zirconia
Zr	Zirconium
ZrH_x	Zirconium hydride

ACKNOWLEDGMENTS

The authors appreciate the support of the Advanced Research Projects Agency-Energy (ARPA-E) program: Modeling-Enhanced Innovations Trailblazing Nuclear Energy Reinvigoration (MEITNER) under contract DE-AR0000977.

1 INTRODUCTION

The study and development of neutron moderators have been central to the realization of fission power from the initial work on purification of the Chicago Pile graphite [1]. Since that early work, a wide range of reactor types, generally classified by coolant, fuel, and moderator type, have been developed by the international community. Recently, compact thermal fission reactors (i.e., microreactors, small modular reactors) are of increased interest for their potential for lower and controlled construction costs, enhanced safety, and portability to remote areas. The compact nature of these reactor cores by definition requires high-performance moderator materials. Given its equivalent mass to neutron, its low neutron absorption cross section, and its high neutron scattering cross section, hydrogen efficiently slows down fast neutrons. Therefore, hydrogen-bearing materials (e.g., water, metal hydrides) have been widely selected as candidates for moderators in various thermal nuclear reactors [2, 3]. The use of water as a high-temperature moderator material has been restricted by the requirement for extremely high pressure. In contrast, metal hydrides are uniquely suitable for use as high-temperature moderators [3, 4]. Figure 1 shows the effective reactivity as a function of fuel volume fraction of a 1-meter reflected spherical reactor core. It is apparent that only hydrogen-bearing moderators yield increased reactivity when fuel is displaced. Therefore, the use of hydrogen-bearing moderators will enable a spatially efficient reactor core design with reduced core volume. Because of the neutron transparency of zirconium, as well as the outstanding moderating ratio of hydrogen (the ratio of the macroscopic slowing-down power to the macroscopic cross section for neutron absorption), zirconium hydride (ZrHx) is the most promising high-temperature moderator material. It was employed as the moderator material in multiple historical reactors, such as the Systems Nuclear Auxiliary Power Program [5]; Training, Research, Isotopes, General Atomic research reactors [6]; and nuclear thermal propulsion reactors [7]. In these cases, ZrH_x was purposefully used as the matrix for fissile materials in nuclear fuel applications. The most common type of hydride fuel consists of metallic uranium dispersed in a ZrH_x matrix with a nominal composition of U(30 wt %)-$ZrH_{1.6}$. Higher power density, high moderator density inherent to the fuel, large prompt negative fuel-temperature reactivity feedback, and higher thermal conductivity are attractive attributes of this class of fuels [6]. In addition, the other metal hydride, yttrium hydride, was also conceived as an excellent moderator material, and had superior thermal stability to ZrHx, although the neutron absorption cross section of yttrium is higher than that of zirconium [8, 9]. It has been selected as the candidate moderator material for the Transformational Challenge Reactor [10].

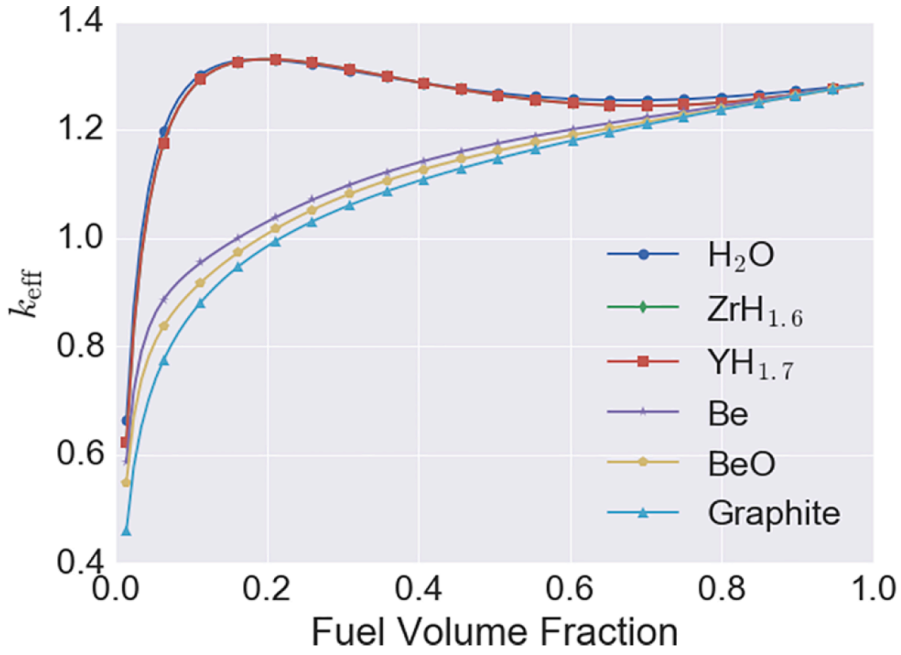

Figure 1. k_{eff} *as a function of fuel volume fraction for a 1-meter reflected spherical reactor core showing only hydrogen-bearing moderators yield increased reactivity when fuel is displaced [10].*

A focus of this ARPA-E Meitner project is the development and demonstration of advanced moderators, including a 2-phase composite moderator with either MgO or silicon carbide (SiC) as the host phase containing BeO or ZrHx, as well as the bulk ZrHx moderator. This report is part of the development of the bulk ZrHx moderator. The successful deployment of ZrHx moderator in advanced reactors requires the development of a consistent and affordable production pathway along with implementation of a hydrogen retention solution throughout the reactor life. Fabrication of delta-phase ZrHx is challenging because the absorption of a large amount of hydrogen into alpha-zirconium induces significant volume expansion, and large hydrogen concentration gradient results in cracking. The successful fabrication of bulk delta-phase ZrHx was demonstrated through careful control of the processing temperature and hydrogen flow rate, informed by the well-established thermodynamics of the binary Zr-H system as documented in Milestone Report M2.2.2 [11].

Hydrogen desorption from ZrHx was expected because of the hydrogen dissociation from the H-Zr bonding at elevated temperature. The kinetics of hydrogen desorption from ZrHx was intensively studied [12-14]. Figure 2(a) shows the dehydriding process of a delta-phase $ZrH_{1.62}$ disk at 525°C in vacuum. During the linear temperature ramping process, when the temperature is lower than 250°C, no obvious hydrogen release is observed. Then the hydrogen desorption rate increases with increasing temperature up to the maximum set temperature. In the constant-temperature regime, the hydrogen desorption flux has a tendency to gradually decrease. After around 1 h of continuous hydrogen desorption, a dramatic drop in the hydrogen release rate occurs. As shown in Fig. 2(b), the continuous loss of hydrogen can induce a phase change in which α-zirconium precipitates on the

surface; it gradually dissolves the original δ-ZrHx, a typical moving boundary problem. Therefore, when the material is used in an open environment, the continuous hydrogen loss will convert ZrHx to metal zirconium, resulting in complete loss of the moderating capability. On the other hand, if it is used in a sealed environment, although hydrogen desorption will still occur, the released hydrogen will lead to the increase in the hydrogen partial pressure of the open volume. Finally, equilibrium will be established when the hydrogen partial pressure is equal to the equilibrium H_2 pressure of the $ZrH_{x'}$ (the hydrogen concentration of ZrHx is changed because of the loss of hydrogen) at the application temperature.

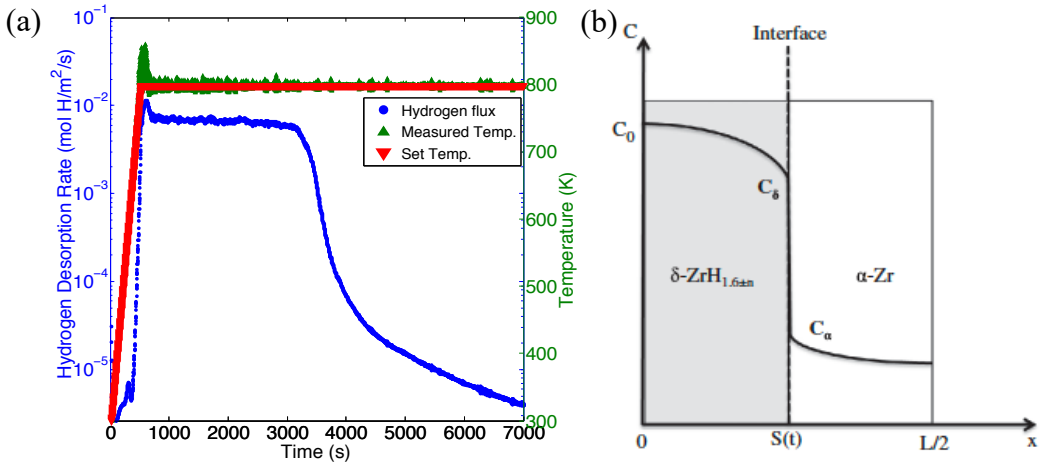

Figure 2 (a). Hydrogen desorption flux from a $ZrH_{1.62}$ disk (surface area of 18 mm^2, thickness of 0.6 mm) as a function of time during heating process. (b) Schematic illustration of the concentration profile during the dehydriding process [13].

The long-term operation of advanced reactors using ZrHx as a moderator requires careful management of hydrogen retention, as ZrHx dissociates to metal zirconium and hydrogen at elevated temperatures. Flowing hydrogen at a specific pressure is sufficient to maintain the H/Zr atomic ratio in the initial ZrHx material during lab testing; however, that strategy will require careful consideration in real reactor applications. Thermal gradients across the core and the ZrHx moderator are expected because of the non-uniform reactor power distribution. Under the same environmental hydrogen pressure, the low-temperature zones of the hydride will have high hydrogen content due to additional absorption of hydrogen from the flowing gas. This process is well understood based on the pressure-composition-temperature map of the binary Zr-H system. It is unclear how the redistribution of the hydrogen within the hydride will impact the neutronic performance of the ZrHx moderator; that issue will need to be assessed based on the specific design of the reactor core. Moreover, the exposure of a metal hydride to flowing gas has the potential to introduce oxygen into the reactor core. As the affinity of zirconium for oxygen is insatiable, and the oxygen solubility in zirconium is high, the ZrHx moderator will act as an oxygen absorber during the operation, imposing additional safety and performance concerns. A more practical method to mitigate hydrogen loss is to develop a cladding as barrier. Cladding materials having lower neutron absorption cross sections and lower permeability to hydrogen are necessary for long-term use in high-temperature nuclear reactors. The down-selection of cladding materials for a ZrHx moderator will also consider chemical

compatibility with ZrH_x, radiation stability, and fabricability. In this report, we assess two candidate cladding materials, FeCrAl and SiC, in detail.

2 REACTOR PHYSICS ANALYSIS OF CLADDING MATERIALS FOR ZIRCONIUM HYDRIDE MODERATOR

The Resource Team (RT) performed a systematic evaluation of eight cladding materials molybdenum, niobium, tantalum, FeCrAl, aluminum oxide [Al_2O_3], 8% yttria-stabilized zirconia [YSZ], SiC, and Inconel 690) in terms of the neutronic effect by using a high-temperature gas-cooled reactor (HTGR) model developed by Prof. N. Brown at University of Tennessee, Knoxville [15, 16]. Each cladding was evaluated at different moderation levels to determine the optimal moderation. The best case for each cladding was then depleted for a standard cycle (1500 effective full power days [EFPD]) to determine its cycle length.

2.1 Criticality evaluation of selected cladding materials

ZrHx has a significantly higher moderating power compared with the conventional graphite moderator of an HTGR, so it is expected that the optimal ratio of fuel to moderator will be larger than for a conventional HTGR. Therefore, voids were added to the moderator/clad mixture to reduce the amount of moderator present in the reactor. This void was accounted for via a density adjustment; if the volume fraction of void was 20% the density of the moderator was reduced by 20%. In a typical HTGR model there are 210 fuel pins. If each of those pins had a cladding 1 mm thick, the volume fraction of cladding in the cladding–matrix mixture would be 6%. Therefore, 6% was the minimum cladding volume fraction that was investigated. The void fraction was investigated in 10% increments from 10% to 90%. Table 1 shows the volume fractions of the clad, void, and moderator that result in the highest initial reactivity. It is desirable to have high reactivity at the beginning of the cycle so the cycle length will be as long as possible. Table 1 shows that molybdenum and tantalum would not be good claddings, as even at the beginning of the cycle, with a very thin clad layer the configurations are subcritical. Based on the calculated reactivities, niobium and FeCrAl are two promising candidate cladding materials in the category of metallic claddings; and MgO and SiC are two excellent cladding candidates in the category of ceramic claddings.

Table 1. Optimal volume fractions of components that result in the highest reactivity.

Cladding materials	Volume fraction of cladding	Volume fraction of void	K_{inf}
Mo	6	70	0.95030
Nb	6	70	1.17424
Ta	6	0	0.08513
Al_2O_3	6	80	1.46846
SiC	6	80	1.48214
YSZ	6	80	1.46902
FeCrAl	6	80	1.12779

Inconel690	6	80	1.11607
MgO	7	80	1.48895

2.2 Cycle length calculation

The six cladding candidates that had $k_{inf} > 1$ at the beginning of the cycle were depleted to 1500 EFPD to determine at which point each design would become subcritical. Figure 3 shows that while the ceramic cladding candidates—YSZ, Al_2O_3, and SiC—are critical for the whole standard cycle length of 1500 EFPD, the metallic cladding materials all have much shorter cycle lengths between 400 and 600 EFPD.

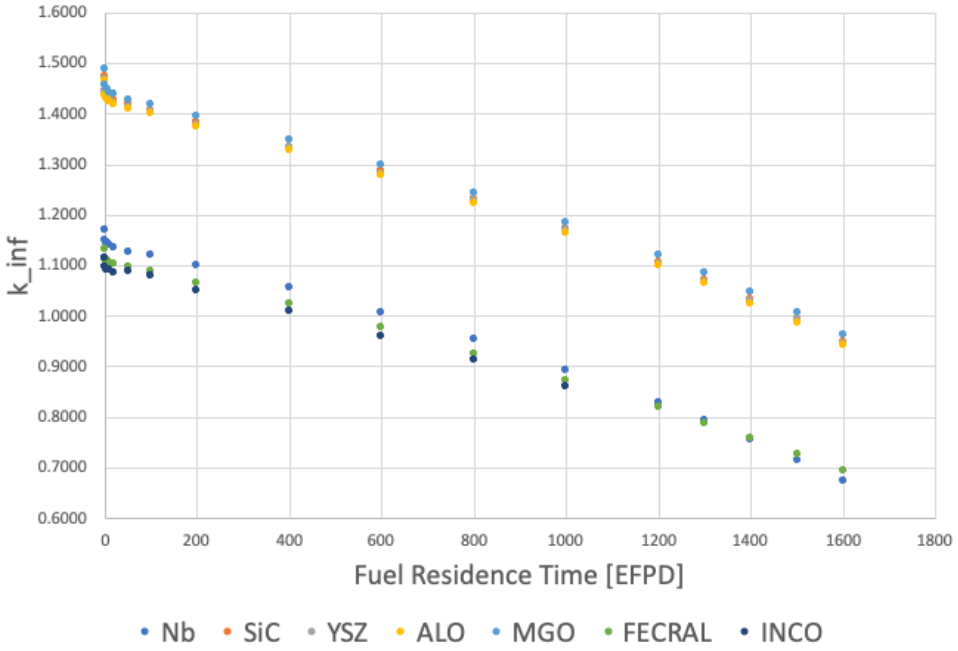

Figure 3. HTGR cycle length of the evaluated cladding materials.

2.3 Neutron flux spectra

Figures 4 and 5 show the beginning-of-cycle and the end-of-cycle (1500 EFPD) neutron flux normalized per lethargy for different cladding material options. The normalized flux per unit of lethargy represents the population of neutrons of a given energy within the moderator. The thermal neutron flux is high owing to the high moderating power of ZrHx. In Fig. 5, tantalum and molybdenum are not included as their beginning-of-cycle k_{inf} values were too low to deplete for a full cycle. The neutron flux spectra are tallied in the moderator matrix and not the fuel matrix or coolant channels.

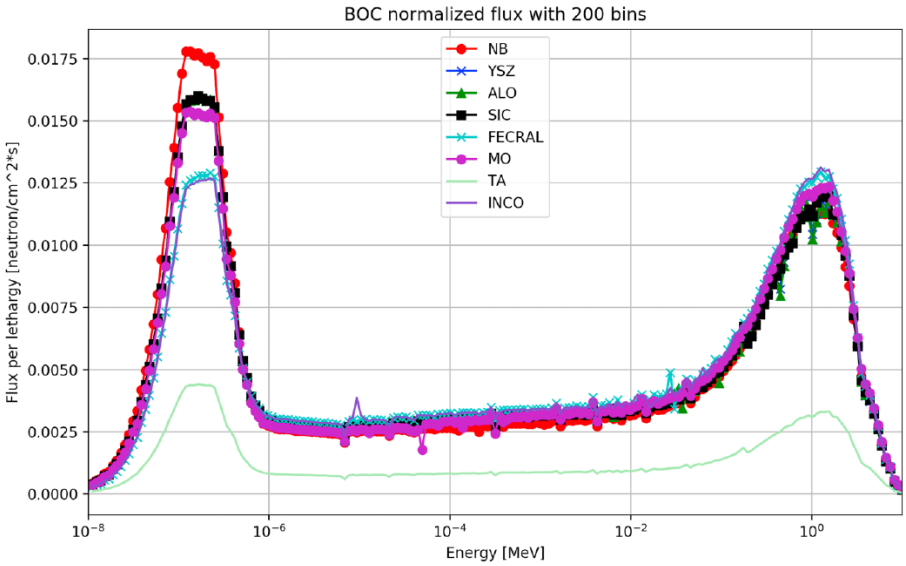

Figure 4. Beginning-of-cycle neutron flux normalized per unit of lethargy.

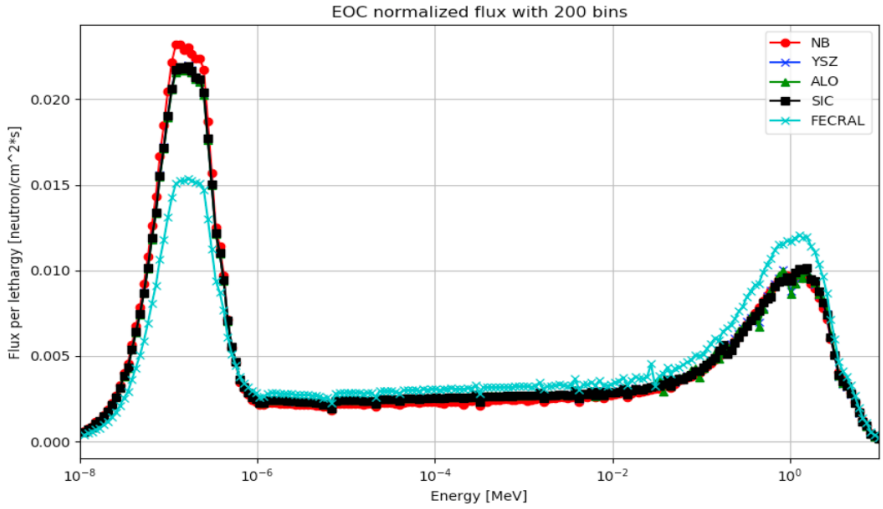

Figure 5. End-of-cycle neutron flux normalized per unit of lethargy.

The neutronics analysis of candidate cladding materials provides the basis for selecting appropriate cladding materials for further investigation. It is apparent that two metallic materials, i.e., niobium and FeCrAl, and all four ceramic materials exhibit good neutronic performance. Because of the limited project time, we will focus on the cladding materials that have been well studied in the nuclear field. Thanks to the intensive research and development (R&D) activities associated with accident-tolerant fuel (ATF) cladding for light water reactors (LWRs) in the past 8 years, and the ongoing fusion materials research, the nuclear community has accumulated abundant knowledge regarding the performance of FeCrAl and SiC in the hostile nuclear environment. Therefore, the application of these two materials as cladding for ZrHx moderator is further discussed in the following sections, including hydrogen permeability, chemical compatibility with ZrH_x, radiation stability, and fabricability.

3 FECRAL CLADDING

Iron-based alloys, both austenitic and ferritic steels, have been used as nuclear fuel cladding since 1951 [17]. Because of their susceptibility to stress corrosion cracking (SCC) and the drive to achieve higher burnups and better economics, austenitic stainless steels were soon replaced by zirconium-based cladding. Ferritic steels exhibit better SCC resistance but are never doped for use in commercial LWRs. As a near-term strategy to improve the accident tolerance of nuclear fuels, FeCrAl became a hot topic in ATF R&D because of its exceptional steam oxidation resistance up to near the melting point (~1500°C) [18, 19]. The composition of nuclear-grade FeCrAl has been optimized (10–13 wt % Cr, 5.5–6 wt % Al, 2 wt % Mo for solid solution strengthening, and <0.1 wt % Y to exploit the reactive element effect) to alleviate embrittlement concerns (the formation of α' precipitates under irradiation for FeCrAl containing >14 wt % Cr) while preserving its robust environmental stability. The database for FeCrAl ATF cladding paves the way to evaluating its application as moderator cladding.

3.1 Hydrogen permeability

Hydrogen permeability through FeCrAl was reported by Hu et al. [20]. The chemical compositions of the studied alloys are shown in Table 2. Learning from Fig. 6, it appears that the hydrogen permeability of FeCrAl alloys (body-centered cubic crystal structure) is five times greater than that of 304SS (face-centered cubic crystal structure) at 350°C and three times higher at 650°C because of the difference in crystal structure. Compared with pure iron (brown dashed line) [21] , the hydrogen permeabilities of the FeCrAl alloys are 1 to 2 orders of magnitude lower. The black dashed line in Fig. 6 indicates the hydrogen permeability of 406SS ($Fe_{13}Cr_{3.9}Al$), reported in Bell et al. [22], which is very close to that of T35Y2 and T54Y2; the similarity in permeability is attributed to their similar composition. APMT with higher chromium and aluminum contents has smaller hydrogen permeability compared with T35Y2 and T54Y2. Considering the potential application of these materials as fuel claddings, the hydrogen permeabilities of Zircaloy-2 and Zircaloy-4—the current fuel cladding materials for boiling water reactors and pressurized water reactors, respectively—are also plotted in the same figure. As expected, the results indicate that hydrogen permeation in the FeCrAl alloys is nearly 2 orders of magnitude higher. In summary, the hydrogen permeation through FeCrAl alloys is high, preventing its direct application as ZrHx cladding. However, as discussed in Hu et al. [20], the hydrogen release through FeCrAl can be mitigated through surface oxide films, which could be engineered during fabrication or grown in situ during operation. The alloy Al_2O_3 is an excellent hydrogen barrier, as manifested by its extremely low hydrogen permeability, nearly 9 orders of magnitude lower than that of bare FeCrAl. However, the stability of the oxide film on the surface and its compatibility with ZrHx and the reactor coolant needs further investigation.

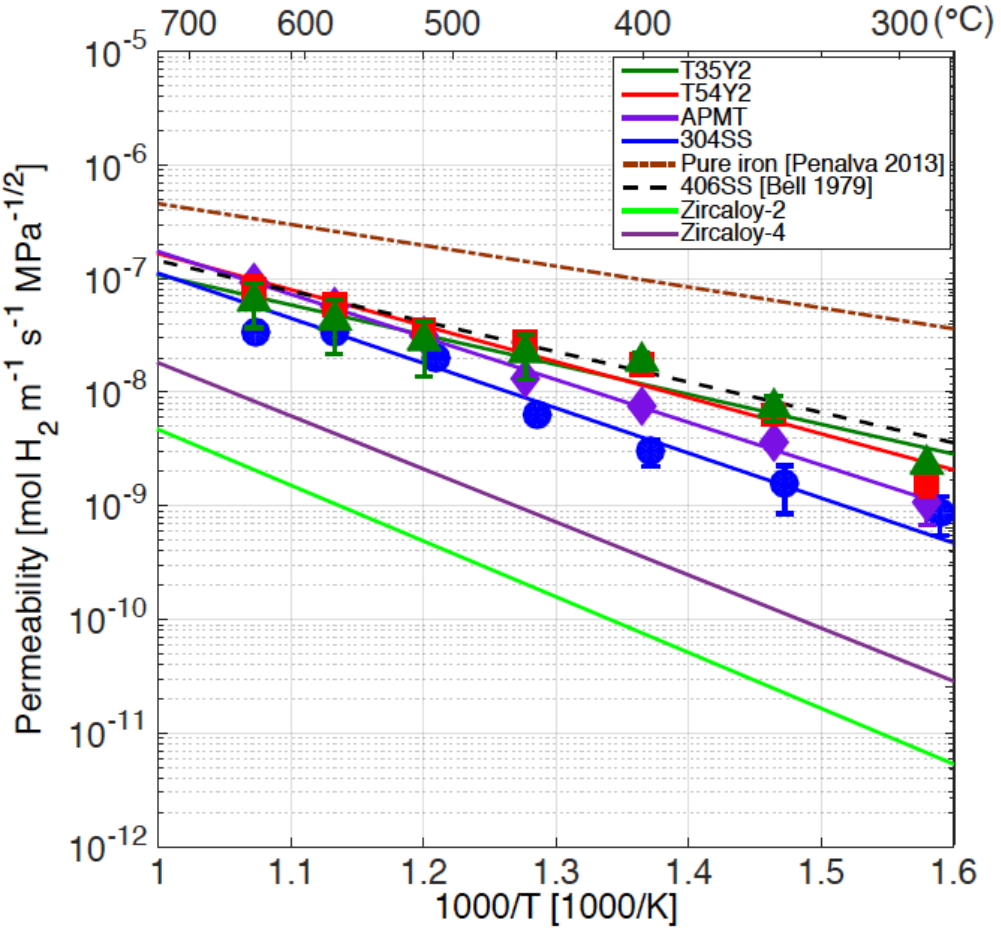

Figure 6. Arrhenius plot of the hydrogen permeability for T35Y1, T54Y2, APMT, 304SS, 406SS, Zircaloy-2, Zircaloy-4, and pure iron over a temperature range from 350 to 650°C [20].

Table 2. Chemical compositions (wt %) of the alloys used for permeation tests [20].

Materials	Chemical compositions (wt%)								
	Fe	Cr	Al	Y	Mo	Mn	C	S	Si
304SS	Bal.	18.35	–	–	0.14	1.31	0.062	0.02	0.57
T35Y2	Bal.	13.15	4.44	0.12	–	<0.01	0.002	0.0003	0.01
T54Y2	Bal.	15.06	3.93	0.12	–	<0.01	0.002	0.0003	0.02
APMT	Bal.	21	5	–	3	<0.4	0.05	–	<0.7

3.2 Chemical compatibility of FeCrAl with ZrHx

One important aspect of the FeCrAl-ZrHx moderator assembly is the chemical compatibility of these two materials that are in contact. A thermodynamics simulation was performed to evaluate the possible formation of chemical compounds for the Fe-Cr-Al-H-Zr system as a function of temperature. First, a Fe-Cr-Al-H-Zr database was compiled based on the Scientific Group Thermodata Europe pure element and compound database

[23]. The Fe-Cr-Zr, Fe-Cr-Al, Al-Zr, and Zr-H subsystems were modeled based on literature data [24-26]. The calculation was performed using Pandat [27]. The composition of the studied system was fixed at x(Fe)=0.25, x(Cr)=0.03, x(Al)=0.02, x(Zr)=0.27, and, x(H)=0.43. Figure 7 shows the mole fraction of phases in equilibria of the Fe-Cr-Al-H-Zr system as a function of temperature. In the temperature regime of interest, 400~650°C, FeCrAl can react with ZrH2_H to form Laves_C15 (i.e., $[Fe,Cr]_2Zr$ phase). However, whether the reaction will happen and how far this reaction can go are dependent upon the elemental diffusivity in this temperature range. Experimental results found negligible amounts of stable chemical compounds at interfaces, suggesting sluggish diffusion kinetics at this temperature. The hydrogen dissociation from ZrHx was expected, as discussed in the Introduction section. A liquid phase was seen when the temperature was greater than 960°C, setting the maximum application temperature of FeCrAl as a ZrHx moderator cladding. Note that this analysis exhibited only the formation of stable chemical compounds when these five elements were mixed together; the kinetics of the reactions is still unknown.

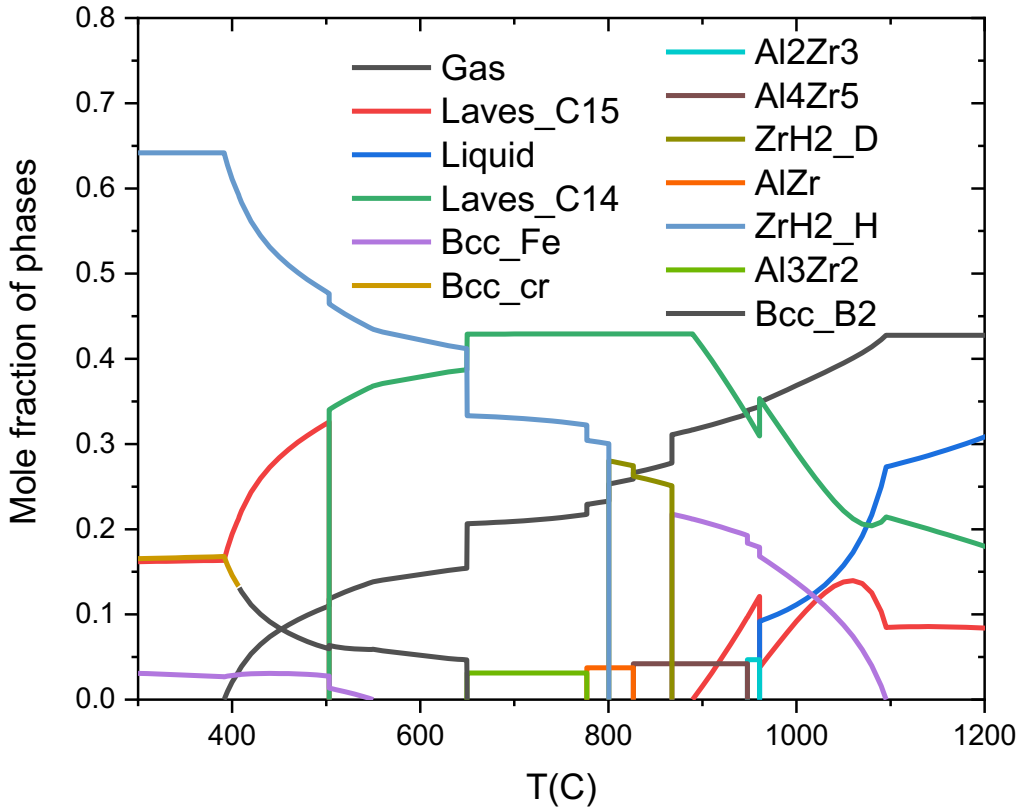

Figure 7. Mole fraction of the formed phases as a function of temperature for the Fe-Cr-Al-H-Zr system

As is discussed in Section 3.1, mitigation strategies are required to prevent hydrogen permeation through FeCrAl. One straightforward method of mitigation is oxidizing FeCrAl in air at high temperature to generate an Al_2O_3 layer on both internal and external surfaces, which serves as the hydrogen barrier. Therefore, it is necessary to evaluate the possible

interaction of Al_2O_3 and ZrHx. A thermodynamics simulation similar to the one mentioned in Section 3.1 was carried out, and the results are shown in Fig. 8. The initial mole fraction ratio of Al_2O_3 and $ZrH_{1.6}$ was set to 1:99. The results indicate the formation of AlZr and ZrO_2 in the low-temperature range (670<T<830°C). The evolution of the relative fraction of delta- and epsilon-phase ZrHx was found. It is evident that Al_2O_3 reacts with ZrHx when they are in contact with each other. Therefore, the prevention of hydrogen loss cannot be dependent on the internal Al_2O_3 surface. The Al_2O_3 film on the external surface of the FeCrAl will act as a hydrogen barrier.

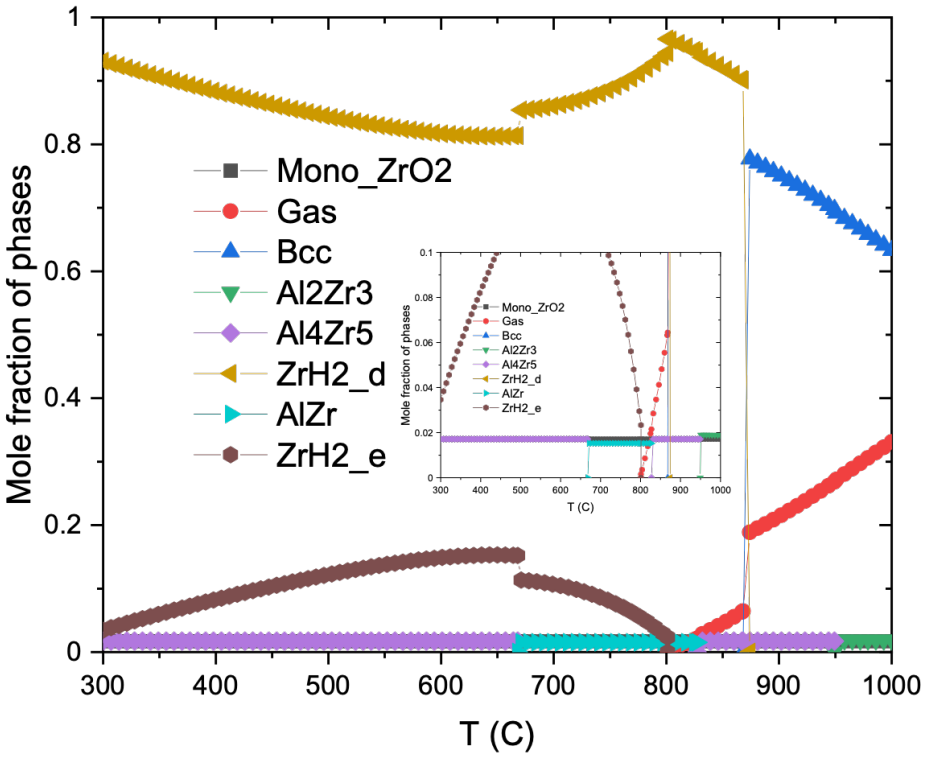

Figure 8. Mole fraction of the formed phases as a function of temperature for the Zr-H-Al-O system.

3.3 Radiation stability

The irradiation response of FeCrAl alloys has been well studied. An up-to-date review of various properties and behavioral aspects of FeCrAl alloys for the ATF cladding application is available in two handbooks by Field et al. [28, 29]. The primary defect features found in neutron-irradiated FeCrAl alloys are voids, dislocation loops, and precipitates. FeCrAl, one class of ferritic steels, has excellent swelling resistance. The primary swelling study for FeCrAl alloys was completed by Little and Stow on a 14.5 wt % Cr-4.18 wt % Al FeCrAl alloy with an initial grain size of ~100μm. This alloy was irradiated up to 23 displacements per atom (dpa) in the temperature range of 380~615°C within the Dounreay Fast Reactor [30]. The void swelling for all irradiation conditions was shown to be within the detection limit (0.1%) of the technique. More recent work on

commercial FeCrAl alloys and Oak Ridge National Laboratory (ORNL) model alloys irradiated in the temperature range of 334~382°C up to 1.8 dpa have shown similar swelling resistance with no observations of voids or cavities [31], although the irradiation conditions are irrelevant to the application environment of a FeCrAl-ZrHx moderator. Preliminary studies of neutron-irradiated ORNL model FeCrAl alloys using materials test reactors have linked the observed radiation-induced hardening to both dislocation loop formation and precipitates. Neutron and ion irradiation in the temperature range of 334°C to 384°C at up to 2.5 dpa have been shown to produce a mixed population of dislocation loops with either a Burgers vector of a/2<111>, which can be either interstitial or vacancy in nature, or a<100> with an interstitial nature [31]. The primary focus of precipitation studies in irradiated FeCrAl alloys is the precipitation of the Cr-rich α' phase within the α matrix.

3.4 Fabricability

The fabrication of FeCrAl tubes has been well demonstrated in ATF R&D. A vacuum melt process is suggested for nuclear-grade FeCrAl alloy heat production to obtain the target alloy composition and avoid potential contamination of unintended/undesired elemental additions, such as nitrogen. The as-cast ingot typically exhibits a dendritic structure with compositional segregation at the dendrite arm spacing. Thermomechanical treatment at elevated temperature is necessary to break the solidification microstructure before any production process begins. The FeCrAl tube production process for moderator cladding application includes three major steps: (1) heat production, (2) master bar production, and (3) tube reduction. A columnar-shape cast ingot is made by a vacuum induction melt process, followed by hot isostatic pressing to ensure compositional homogenization and eliminate potential internal defects that may form during the solidification process. The ingot is machined into the necessary size for the master bar production step, either through a hot extrusion process or hot forging. The process parameters (e.g. process temperatures, area reduction ratio) need to be defined to control the microstructure (e.g., refined grain structure) and provide sufficient deformability of the material in the subsequent tube reduction process. The master bars are gun-drilled to make master tubes, and then either tube drawing or pilgering is applied in either a cold or warm condition (up to ~300°C). The size of the die and mandrel are selected to control the area reduction in each pass so that it does not exceed the limit of the material deformability, to avoid premature failure (e.g. cracks, necking). In combination with inter-pass annealing, the reduction process targets exceeding an 80% total wall-thickness reduction to ensure sufficiently homogeneous deformation and control the uniform grain structure in the final tube products [28, 29]. Joining of FeCrAl alloys has been studied using gas tungsten arc welding, gas metal arc welding, laser beam welding, electron beam welding, and pressure resistance welding. Hermetic FeCrAl tubes have been successfully fabricated by welding thin-walled tubes of FeCrAl alloys to caps made of the same material [32].

In summary, FeCrAl alloys are excellent candidate cladding materials for a ZrHx moderator given their proven radiation stability, acceptable compatibility with ZrHx, and industrially established fabricability. The relatively high hydrogen permeability is

manageable by introducing a thin layer of an A_2O_3 hydrogen permeation barrier on the external surface.

4 SiC-BASED CLADDING

Silicon carbide and the continuous fiber–reinforced SiC matrix composite (SiC/SiC) technology are considered for use in the current and next generation nuclear power systems. Specific applications under consideration include fuel assembly components, core internal and other in-vessel components of LWRs [33]; control rod drive components and hanger straps for high-temperature and very-high-temperature reactors; cladding and other components of gas fast reactors, and so on. [34-36]. A particular application considered for SiC/SiC composite is ATF cladding for LWRs because of its outstanding benefits, including exceptional radiation resistance and outstanding passive safety features in beyond-design-basis severe accident scenarios. As a leading option for ATF cladding, the performance of SiC/SiC composite in a nuclear environment has been intensively studied, which motivates study of its application as a ZrHx moderator cladding.

4.1 Hydrogen permeability

Bulk SiC is considered an effective hydrogen barrier because of its extremely low hydrogen permeability, like that of other ceramics, as shown in Fig. 9. Nuclear-grade SiC/SiC composites are typically fabricated using chemical vapor infiltration (CVI), which employs a stoichiometric and crystalline beta-phase SiC matrix, near-stoichiometric crystalline SiC fibers, and a monolayer carbon interphase or multilayer carbon/SiC interphase. CVI is considered a low-temperature processing method for the fabrication of SiC matrix composites, with the benefits of minimal process-induced damage to the fibers and reduced residual thermal stress [34]. However, CVI composites inherently consist of fabric layup architectures made up of small, elongated inter-fiber pores with more macroscopic inter-bundle pores. The porosities of as-fabricated CVI SiC/SiC composites are usually in the range of 15~20%, and it is challenging to reach very low porosity levels. Therefore, a chemical vapor deposition (CVD) SiC coating is typically applied inside and/or outside the cladding, depending on the particular material design, to provide the required gastightness. Although SiC/SiC composites undergo pseudo-ductile facture rather than brittle failure, micro-cracking may occur during the process or under the expected in-pile stress state [37], which can lead to a loss of hermeticity. Significant R&D activity is ongoing to investigate the hermeticity of SiC/SiC composite when it is subjected to a real nuclear environment.

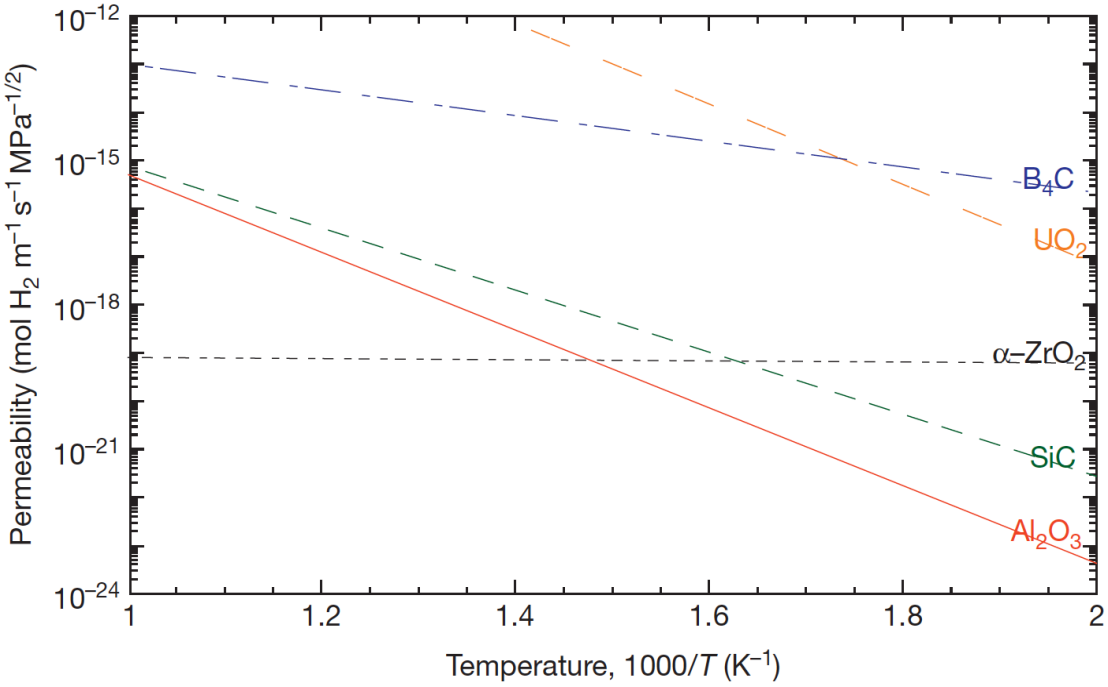

Figure 9. Arrhenius plot of the hydrogen permeability for SiC and selected ceramic materials [38] .

4.2 Chemical compatibility of SiC with ZrHx

Following the same method introduced in Section 3.2, a thermodynamic calculation was performed to evaluate the possible interactions in a Si-C-H-Zr system. Stable phases of SiZr and ZrC are expected at temperatures lower than 1000°C, implying the interaction of Zr and SiC. It is unclear whether this will be a showstopper, as the kinetics of this interaction is unknown. The SiZr or ZrC formed on the surface could work as a barrier to prevent further interactions and hydrogen desorption. More efforts are needed to investigate this topic.

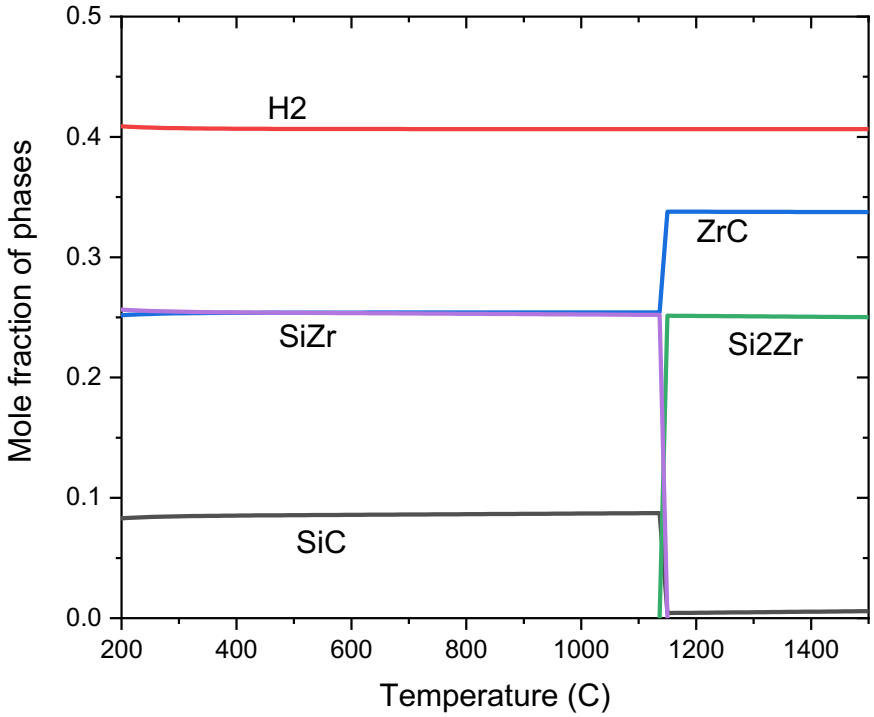

Figure 10. Mole fraction of the formed phases as a function of temperature for the Si-C-H-Zr system

4.3 Radiation stability

The neutron irradiation effect of CVD SiC has been well studied and documented, as summarized in Snead et al. [39]. One important radiation-induced degradation of SiC is swelling. Swelling at temperatures between the amorphization threshold (~150°C) and the onset of the radiation-induced void contribution (~1000°C) is referred to as "transient swelling." The transient swelling of SiC accumulates at a rate depending on the irradiation temperature and dose until it reaches a saturation value that is a function only of temperature. Approximate magnitudes of saturation volumetric swelling are ~2% at 300°C and ~0.7% at 800°C [39]. Recent experiments showed that this saturation persists at least up to a dose of ~70 dpa [36]. The neutron irradiation effects on the thermomechanical properties are also well documented [39].

Significant efforts have been committed to understanding irradiation effects on SiC/SiC composite [34, 40]. Obviously, the properties of a composite material are determined by the properties of its constituents—the matrix, fiber, and interface—and the constitutive laws that are in many cases for the specific reinforcement architecture. The matrix material for SiC/SiC composite is high-purity beta-phase SiC, the neutron irradiation effects on which are well understood [39]. Near-stoichiometric beta-phase SiC fibers are considered to behave in a manner similar to high-purity CVD SiC, represented by Hi-Nicalon Type S and Tyranno-SA3. The fiber/matrix interfacial properties depend significantly on the residual stress. The differential swelling among constituents will generate a complex stress

state at the interface and might result in debonding. The effects of neutron irradiation on SiC/SiC composite are summarized in Katoh et al. [34].

4.4 Fabricability

CVI SiC/SiC composite is a mature technology that has already demonstrated scale components with reasonable reproducibility up to large dimensions [41]. General Atomics became capable of producing ~1-m-long SiC/SiC composite tubes through a CVI process with adequate straightness, wall thickness uniformity, roundness, and surface roughness. In SiC/SiC composite ATF cladding development, end plug technology is being developed. Various technologies for joining SiC-based materials have been studied, developed, and evaluated [42]. However, these joining techniques all involve high-temperature processing, making them inappropriate to seal SiC-based tubes containing ZrHx, as significant hydrogen loss will occur.

The RT identified welding and 3D printing using a high-power ultrashort pulsed laser as the most attractive high-risk, high-potential technologies. The RT identified a small business named PolarOnyx Inc. (San Jose, CA) as the supplier of the technology. The initial technical approach to testing was laser welding of SiC in the ambient. The outside supplier attempted femtosecond fiber laser welding in air of the two CVD SiC plates supplied by the RT. The results indicated unacceptable amounts of silicon oxide were produced during the processing, as previously reported. Given the unknown magnitude of the technical challenge associated with searching for the appropriate process condition space for this laser welding approach, the RT decided to shift the focus to the 3D printing of SiC cladding. In this approach, the femtosecond laser technology will be used in combination with conventional laser powder bed fusion 3D printing. The primary objective of the initial attempt is to determine the viability of the powder bed 3D printing approach for producing SiC articles of reasonable quality without excessively heating the metal hydride pellet that is to be cladded in. The initial attempt using a high-purity SiC feedstock powder precursor was successful in printing small cylinders (Fig. 11).

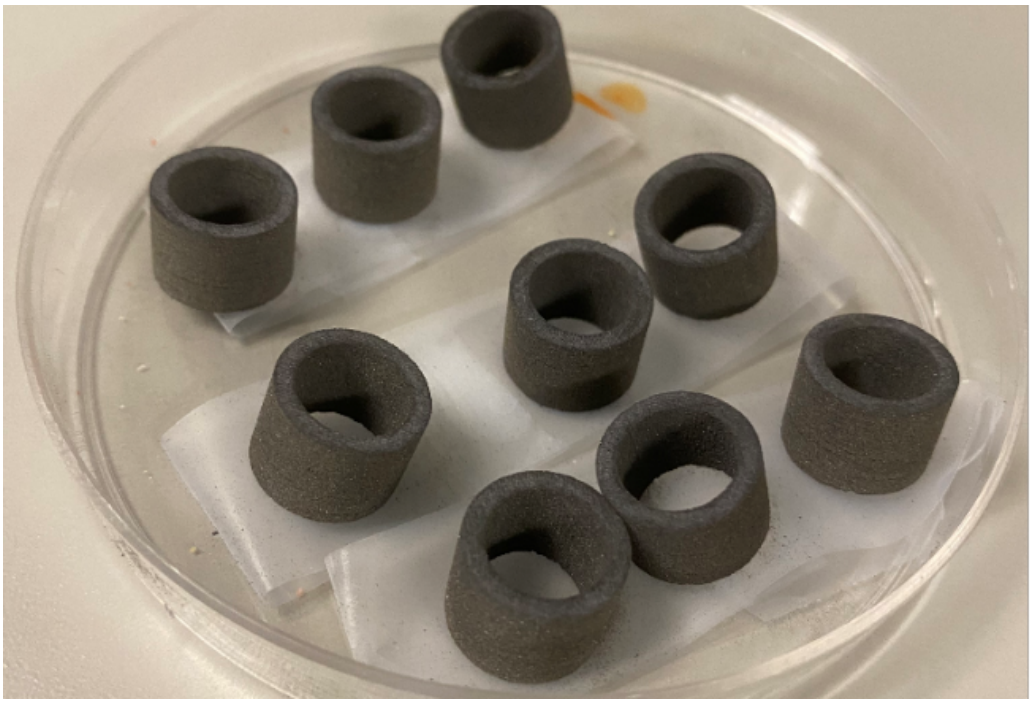

Figure 11. The first-generation SiC samples fabricated by laser-powder bed fusion additive manufacturing. The cylinders are of 0.5 in. (12.7 mm) outer diameter.

X-ray diffraction (XRD) analysis indicated that the printed article consisted predominantly of multiple phases of hexagonal SiC: 6H, 4H, and 15R. An example is shown in Fig. 12. XRD also indicated the presence of metallic silicon at a significantly increased abundance (estimated 3.5 to 12 mass %) compared with that in the feedstock powder (<1 mass %). This finding indicated that SiC decomposition was involved in the laser additive manufacturing (AM) mechanism. Additional details are being examined for microstructures and microchemistries of the AM SiC samples processed under varied conditions to acquire further insight.

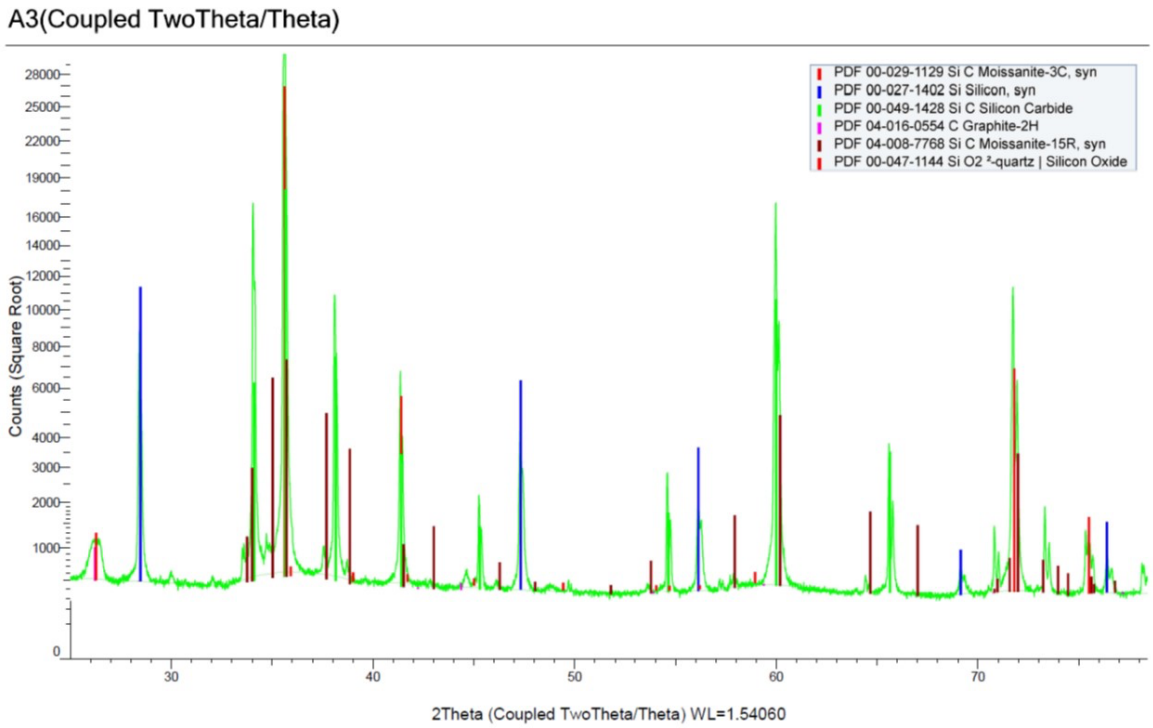

Figure 12. X-ray diffraction spectrum taken from Specimen A3 of femtosecond laser-manufactured SiC, indicating the presence of multiple SiC polytypes and metallic silicon.

Porosity analysis based on the bulk and immersion densitometries indicated roughly ~40% open porosity for all the AM SiC articles. Although the results of the gas permeation measurements are not yet available, it is anticipated that improved densification will be needed to ensure adequate clad tightness against hydrogen permeation.

The path forward for this AM SiC effort can be summarized as follows:

- Perform detailed examinations of the current batch of AM SiC samples to acquire knowledge and insight into the exact consolidation mechanism.
- Examine the properties and microstructures of the final deliverable AM SiC samples from the outside supplier.
- Develop a technical plan toward improving the phase purity and gas-tightness of SiC produced through AM routes.

More effort will be invested in exploiting this high-risk, high-potential technology to produce hermetic SiC-based ZrHx moderator cladding.

5 SUMMARY

In this report, detailed assessments of FeCrAl and SiC-based cladding for a ZrHx moderator are presented with respect to the neutronics, radiation stability, hydrogen

permeability, chemical compatibility with ZrHx, and fabricability. The analysis indicated the following:

- FeCrAl alloys are excellent candidate cladding materials for a ZrHx moderator given their proven radiation stability, acceptable compatibility with ZrHx, and industrially established fabricability. The relative high hydrogen permeability is manageable by introducing a thin layer of an A_2O_3 hydrogen permeation barrier on the external surface.

- The SiC-cladded ZrHx moderator is promising because of its outstanding neutronics performance, excellent radiation stability, and extremely low intrinsic hydrogen permeability. However, the potential interactions of SiC and zirconium and the challenge in achieving hermetic SiC-based cladding make further investigation necessary.

6 REFERENCES

1. Ang, C., et al., *Fabrication of Two-Phase Composite Moderators as Potential Lifetime Reactor Components*, in *Transactions of the American Nuclear Society - Volume 121*. 2019. p. 1445-1447.
2. Christy, R.F. and A.M. Weinberg, *Light water moderated neutronic reactor.* U.S. Patent, 1946. **App. No. US640100A**.
3. Vetrano, J.B., *Hydrides as neutron moderator and reflector materials.* Nuclear Engineering and Design, 1971. **14**(3): p. 390-412.
4. Mueller, W.M., J.P. Blackledge, and G.G. Libowitz, *Metal Hydrides.* Academic Press New York and London, 1968.
5. Davies, N. and R. Forrester, *Effects of irradiation on hydrided zirconium-uranium alloy NAA 120-4 experiment*. 1970, Atomics International Div.: Canoga Park, CA.
6. Simnad, M., *The U-ZrHx alloy: Its properties and use in TRIGA fuel.* Nuclear Engineering and Design, 1981. **64**(3): p. 403-422.
7. Haslett, R., *Space Nuclear Thermal Propulsion Program*. 1995, Grumman Aerospace Corp.: Bethpage, NY.
8. Hu, X., et al., *Fabrication of yttrium hydride for high-temperature moderator application.* Journal of Nuclear Materials, 2020. **539**: p. 152335.
9. Hu, X. and K.A. Terrani, *Thermomechanical properties and microstructures of yttrium hydride.* Journal of Alloys and Compounds, 2021. **867**.
10. Betzler, B.R., et al., *Transformational Challenge Reactor preconceptual core design studies.* Nuclear Engineering and Design, 2020. **367**.
11. Hu, X., et al., *Fabrication of zirconium hydride with controlled hydrogen loading.* ORNL/SPR-2020/1672, 2020.
12. Terrani, K.A., et al., *The kinetics of hydrogen desorption from and adsorption on zirconium hydride.* Journal of Nuclear Materials, 2010. **397**(1-3): p. 61-68.
13. Hu, X., K.A. Terrani, and B.D. Wirth, *Hydrogen desorption kinetics from zirconium hydride and zirconium metal in vacuum.* Journal of Nuclear Materials, 2014. **448**(1-3): p. 87-95.

14. Ma, M., et al., *Decomposition kinetics study of zirconium hydride by interrupted thermal desorption spectroscopy.* Journal of Alloys and Compounds, 2015. **645**: p. S217-S220.
15. Brown, N.R., M. Todosow, and A. Cuadra, *Screening of advanced cladding materials and UN–U3Si5 fuel.* Journal of Nuclear Materials, 2015. **462**: p. 26-42.
16. Duchnowski, E.M., et al., *Reactor performance and safety characteristics of two-phase composite moderator concepts for modular high temperature gas cooled reactors.* Nuclear Engineering and Design, 2020. **368**.
17. Terrani, K.A., *Accident tolerant fuel cladding development: Promise, status, and challenges.* Journal of Nuclear Materials, 2018. **501**: p. 13-30.
18. Pint, B.A., et al., *High temperature oxidation of fuel cladding candidate materials in steam–hydrogen environments.* Journal of Nuclear Materials, 2013. **440**(1-3): p. 420-427.
19. Terrani, K.A., S.J. Zinkle, and L.L. Snead, *Advanced oxidation-resistant iron-based alloys for LWR fuel cladding.* Journal of Nuclear Materials, 2014. **448**(1-3): p. 420-435.
20. Hu, X., et al., *Hydrogen permeation in FeCrAl alloys for LWR cladding application.* Journal of Nuclear Materials, 2015. **461**: p. 282-291.
21. Peñalva, I., et al., *Influence of the Cr content on the permeation of hydrogen in Fe alloys.* Journal of Nuclear Materials, 2013. **442**(1-3): p. S719-S722.
22. Bell, J.T., J.D. Redman, and H.F. Bittner, *Tririum permeation through clean construction alloys.* Journal of Materials for Energy Systems, 1979. **1**: p. 55-59.
23. Dinsdale, A.T., *SGTE data for pure elements.* Calphad, 1991. **15**: p. 317-425.
24. Dupin, N., et al., *A thermodynamic database for zirconium alloys.* Journal of Nuclear Materials, 1999. **275**(3): p. 287-295.
25. Yang, Y., et al., *Thermodynamic modeling and experimental study of the Fe–Cr–Zr system.* Journal of Nuclear Materials, 2013. **441**(1-3): p. 190-202.
26. Wang, T., Z. Jin, and J. Zhao, *Thermodynamic assessment of the Al-Zr binary system.* Journal of Phase Equilibria, 2001. **22**: p. 544-551.
27. *https://computherm.com/software.*
28. Field, K.G., et al., *Handbook on the Material Properties of FeCrAl Alloys for Nuclear Power Production Applications.* ORNL/TM-2017/186, 2017.
29. Field, K.G., et al., *Handbook on the Material Properties of FeCrAl Alloys for Nuclear Power Production Applications.* ORNL/SPR-2018/905, 2018.
30. Little, E.A. and D.A. Stow, *Void-swelling in irons and ferritic steels: II. An experimental survey of materials irradiated in a fast reactor.* Journal of Nuclear Materials, 1979. **87**: p. 25-39.
31. Field, K.G., et al., *Radiation tolerance of neutron-irradiated model Fe–Cr–Al alloys.* Journal of Nuclear Materials, 2015. **465**: p. 746-755.
32. Rebak, R.B., *Iron-chrome-aluminum alloy cladding for increasing safety in nuclear power plants.* EPJ Nuclear Sciences & Technologies, 2017. **3**.
33. Zinkle, S.J., K.A. Terrani, and L.L. Snead, *Motivation for utilizing new high-performance advanced materials in nuclear energy systems.* Current Opinion in Solid State and Materials Science, 2016. **20**(6): p. 401-410.

34. Katoh, Y., et al., *Continuous SiC fiber, CVI SiC matrix composites for nuclear applications: Properties and irradiation effects.* Journal of Nuclear Materials, 2014. **448**(1-3): p. 448-476.
35. Katoh, Y. and K.A. Terrani, *Systematic Technology Evaluation Program for SiC/SiC Composite-based Accident-Tolerant LWR Fuel Cladding and Core Structures.* ORNL/TM-2015/454, 2015.
36. Katoh, Y., et al., *Dimensional stability and anisotropy of SiC and SiC-based composites in transition swelling regime.* Journal of Nuclear Materials, 2018. **499**: p. 471-479.
37. Ben-Belgacem, M., et al., *Thermo-mechanical analysis of LWR SiC/SiC composite cladding.* Journal of Nuclear Materials, 2014. **447**(1-3): p. 125-142.
38. Causey, R.A., R.A. Karnesky, and C. San Marchi, *Tritium Barriers and Tritium Diffusion in Fusion Reactors*, in *Comprehensive Nuclear Materials*. 2012. p. 511-549.
39. Snead, L.L., et al., *Handbook of SiC properties for fuel performance modeling.* Journal of Nuclear Materials, 2007. **371**(1-3): p. 329-377.
40. Deck, C.P., et al., *Characterization of SiC–SiC composites for accident tolerant fuel cladding.* Journal of Nuclear Materials, 2015. **466**: p. 667-681.
41. Naslain, R., *Design, preparation and properties of non-oxide CMCs for application in engines and nuclear reactors: an overview.* Composites Science and Technology, 2004. **64**(2): p. 155-170.
42. Katoh, Y., et al., *Radiation-tolerant joining technologies for silicon carbide ceramics and composites.* Journal of Nuclear Materials, 2014. **448**(1-3): p. 497-511.